

Customized SAM 2 for Referring Remote Sensing Image Segmentation

Fu Rong
School of Computer Science,
Wuhan University
furong@whu.edu.cn

Meng Lan
Hong Kong University of
Science and Technology
eemenglan@ust.hk

Qian Zhang
Horizon Robotics
qian01.zhang@horizon.ai

Lefei Zhang*
School of Computer Science,
Wuhan University
zhanglefei@whu.edu.cn

Abstract

Referring Remote Sensing Image Segmentation (RRSIS) aims to segment target objects in remote sensing (RS) images based on textual descriptions. Although Segment Anything Model 2 (SAM 2) has shown remarkable performance in various segmentation tasks, its application to RRSIS presents several challenges, including understanding the text-described RS scenes and generating effective prompts from text descriptions. To address these issues, we propose **RS2-SAM 2**, a novel framework that adapts SAM 2 to RRSIS by aligning the adapted RS features and textual features, providing pseudo-mask-based dense prompts, and enforcing boundary constraints. Specifically, we first employ a union encoder to jointly encode the visual and textual inputs, generating aligned visual and text embeddings as well as multimodal class tokens. Then, we design a bidirectional hierarchical fusion module to adapt SAM 2 to RS scenes and align adapted visual features with the visually enhanced text embeddings, improving the model’s interpretation of text-described RS scenes. Additionally, a mask prompt generator is introduced to take the visual embeddings and class tokens as input and produce a pseudo-mask as the dense prompt of SAM 2. To further refine segmentation, we introduce a text-guided boundary loss to optimize segmentation boundaries by computing text-weighted gradient differences. Experimental results on several RRSIS benchmarks demonstrate that RS2-SAM 2 achieves state-of-the-art performance.

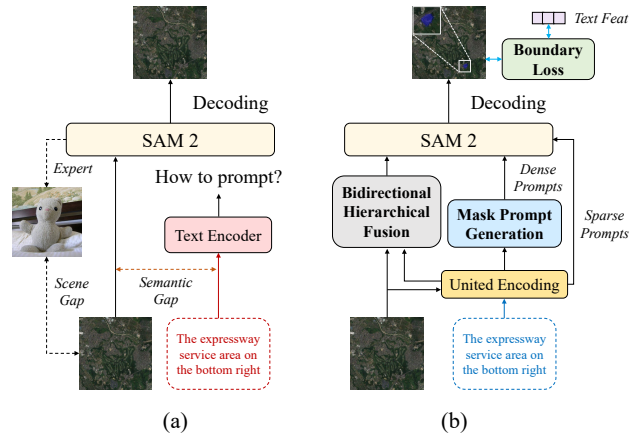


Figure 1. Comparison of two SAM 2 adaptations for RRSIS. (a) vanilla SAM 2, (b) our RS2-SAM 2.

1. Introduction

Referring Remote Sensing Image Segmentation (RRSIS) [19, 38] aims to segment specified targets from aerial images based on textual descriptions. This task extends the capabilities of traditional Referring Image Segmentation (RIS) [17, 30, 35] by addressing the unique challenges inherent to remote sensing images. These challenges include handling diverse spatial scales, interpreting complex scene contexts, and resolving ambiguous object boundaries, which are particularly prevalent in remote sensing scenes.

Recent advances in the Segment Anything Model (SAM) [10] and its variants [9, 32, 41] have demonstrated significant improvements in efficiency and accuracy for promptable segmentation tasks in natural images. These models exhibit powerful segmentation capabilities and robust interactive prompting mechanisms. Notably, SAM 2 [24]

*Corresponding author

incorporates the hierarchical encoder Hiera [26], enhancing its ability to process images with diverse spatial scales. However, despite these advancements, applying SAM 2 to RRSIS remains challenging due to the unique complexities of remote sensing images.

First, while SAM 2 demonstrates strong performance on natural images, its effectiveness diminishes in remote sensing scenes due to the low distinguishability of targets and the limited contrast between foreground and background regions. Furthermore, SAM 2 struggles to effectively utilize spatial information derived from textual descriptions, as illustrated in Fig. 1 (a). Although existing studies have attempted to address these issues, significant room for improvement remains. For example, SAM2-Adapter [1] modifies SAM 2’s encoding process to better adapt to complex scenes. However, this unimodal approach lacks hierarchical information interaction, resulting in an insufficient fine-grained understanding of textual information. Consequently, achieving effective alignment of vision-language information and improving generalization to complex remote sensing scenes remain critical challenges in adapting SAM 2 for RRSIS. **Second**, SAM 2’s inherent lack of textual prompt integration limits its ability to generate prompts that accurately align with given textual descriptions. Previous RRSIS methods, such as RMSIN [19], rely on independent encoding for visual and textual inputs, but such traditional encoder-decoder structures fail to effectively integrate textual information into SAM 2. EVF-SAM [42] addresses this by jointly encoding vision and language features and generating sparse prompts through a multilayer perceptron (MLP), achieving promising results on natural images. However, in remote sensing scenes, sparse prompts alone are insufficient for fine-grained local image understanding, particularly for recognizing subtle and less distinguishable objects. Thus, designing effective prompts based on text description to guide the decoding process remains a critical challenge for adapting SAM 2 to RRSIS. Additionally, objects in remote sensing images often blend with their surroundings, resulting in ambiguous boundaries. Enhancing the distinction between target objects and the background remains an urgent and unresolved issue.

To address these challenges, this paper proposes RS2-SAM 2, a novel RRSIS framework adapted from SAM 2. As illustrated in Fig. 1 (b), our approach focuses on three key aspects: (1) *adapting SAM 2 image features to remote sensing scenes and aligning them with textual features during the image encoding process*, (2) *generating dense prompts for precise segmentation*, and (3) *enforcing boundary constraints throughout training*. Specifically, to adapt SAM 2 to remote sensing scenes and align remote sensing visual features with textual features, we design a bidirectional hierarchical fusion module, which is embedded both within and after the frozen SAM 2 image encoder. Initially,

we utilize a union encoder to jointly encode visual and textual inputs, producing semantically aligned visual and textual embeddings as well as multimodal class tokens. Subsequently, our proposed fusion module hierarchically aligns the visually enhanced textual embeddings with adapted remote sensing visual features in the SAM 2 encoder.

To equip SAM 2 with more precise prompts, we introduce a mask prompt generator. This module integrates jointly encoded visual embeddings and multimodal class tokens to generate a pseudo-mask representing remote sensing target objects. The pseudo-mask is then fed into the SAM 2 prompt encoder as a dense prompt, providing pixel-level positional information to enhance the model’s segmentation capability. Furthermore, we propose a text-guided boundary loss, which computes the gradient values of both the predicted and ground truth masks to better distinguish object boundaries. This loss is dynamically weighted by textual information, effectively constraining the predicted mask boundaries and improving segmentation accuracy.

Experimental results across several RRSIS benchmarks demonstrate the superior performance of our model and the effectiveness of the proposed modules. The primary contributions of this work are outlined as follows:

- We propose the RS2-SAM 2 framework, which adapts the SAM 2 model to the RRSIS task by hierarchically aligning the adapted remote sensing visual and textual features, providing pseudo-mask-based dense prompts, and enforcing boundary constraints.
- We design a bidirectional hierarchical fusion module that adapts the SAM 2 encoder to the remote sensing images and aligns the adapted visual features with textual features during the encoding process.
- We develop a mask prompt generator that leverages multimodal features to produce a pseudo-mask as the dense prompt, offering precise target cues for SAM 2.
- We introduce a text-guided boundary loss to refine segmentation accuracy by constraining boundary consistency.

2. Related work

Referring Remote Sensing Image Segmentation. RRSIS emerges as an important research direction in remote sensing, allowing users to extract geospatial information through natural language queries. Compared to the remote sensing visual grounding (RSVG) [13, 27, 40] task, RRSIS focuses on fine-grained pixel-level analysis rather than region-level identification. However, research in this area remains in its early stages with limited exploration. Yuan et al. [38] pioneer this task by introducing the Ref-segRS dataset and adapting the LAVT [35] framework for remote sensing. To address challenges like small and fragmented targets easily confused with complex backgrounds,

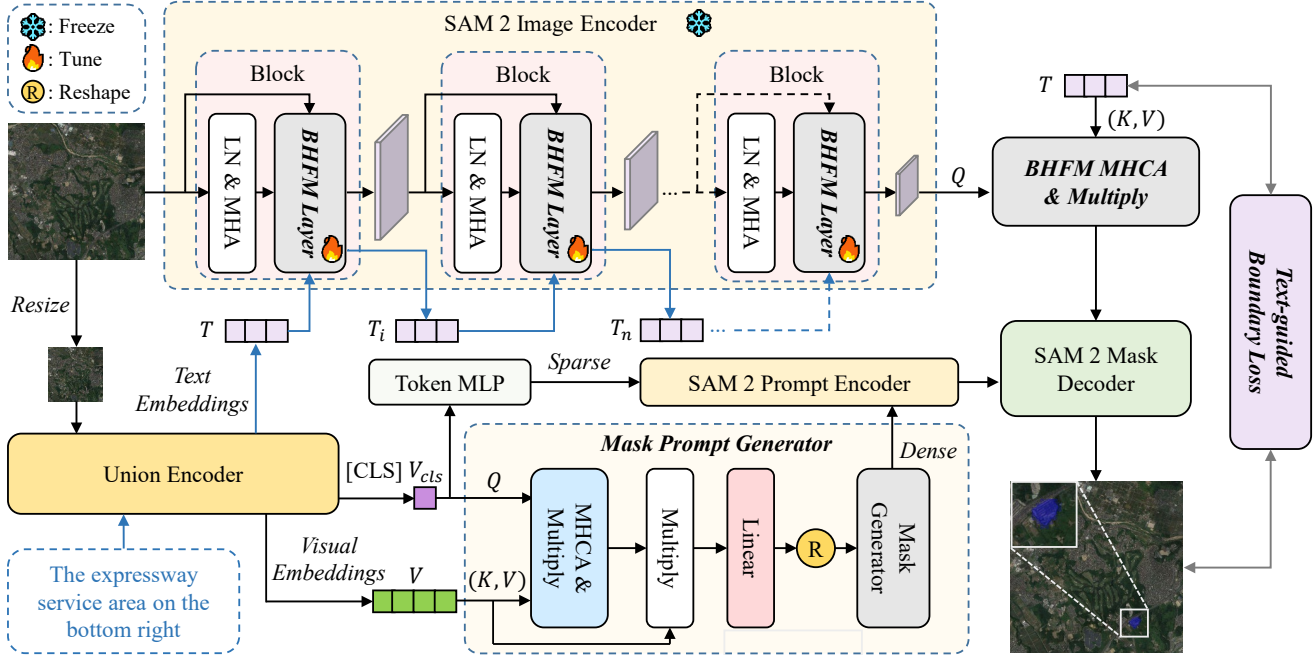


Figure 2. The overview of the proposed RS2-SAM 2 framework. It consists of four key components: the union encoder, the bidirectional hierarchical fusion module, the mask prompt generator, and SAM 2. The union encoder extracts multimodal representations from the input image and text. The bidirectional hierarchical fusion module enhances image features with textual embeddings. The mask prompt generator produces a prior mask as the dense prompt for SAM 2. Finally, SAM 2 generates precise segmentation masks, while the text-guided boundary loss constrains the boundary accuracy of the predicted masks.

they develop a multi-level feature fusion mechanism incorporating linguistic guidance, significantly enhancing small object detection. Subsequently, Liu et al. [19] build upon the RSVG dataset DIOR-RSVG [40] to establish the first large-scale RRSIS dataset, RRSIS-D. They further introduce the RMSIN architecture, which leverages rotational convolution operations to better handle spatial-scale variations and directional complexities in remote sensing images, providing a more robust modeling framework for RRSIS. Building upon RMSIN [19], Lei et al. propose FIANet [14], which focuses more on fine-grained vision-language interaction and adaptive understanding of objects at different scales.

Segment Anything Model. SAM [10] is an interactive model designed to generate non-semantic segmentation masks based on a variety of input prompts. Leveraging large-scale training data, it demonstrates strong generalization across diverse segmentation tasks. SAM has also been widely utilized in multiple domains, including remote sensing image analysis [28], video object tracking [2, 34], and medical image segmentation [3, 39]. To improve its accuracy and efficiency, several optimized versions [32, 41, 43] have been developed. More recently, SAM 2 [24] has been introduced for video segmentation [12, 25], incorporating multi-scale feature encoding to en-

hance segmentation robustness. Despite these advances, SAM remains limited by its lack of linguistic understanding, preventing it from directly handling referring segmentation tasks that require textual guidance. To address this limitation, recent works [11, 23, 33] have explored the integration of multimodal large language models (MLLMs) to enhance SAM’s ability to process language-based instructions. LISA [11], for example, fine-tunes LLaVA [16] to derive hidden embeddings, thereby producing multimodal features for enhanced segmentation. u-LLaVA [33] extends this paradigm by enabling simultaneous region- and pixel-level segmentation through multi-task learning. Due to its lightweight pre-fusion strategy, EVF-SAM [42] leverages joint visual-language encoding to enhance text-driven segmentation prompts, thereby achieving superior segmentation accuracy. However, while these models have demonstrated strong performance on natural images, their effectiveness in complex remote sensing scenes remains limited, highlighting the need for further refinement and adaptation.

3. Method

3.1. Overview

The architecture of the proposed RS2-SAM 2 framework is depicted in Fig. 2. RS2-SAM 2 is composed of four essen-

tial parts: the union encoder, the bidirectional hierarchical fusion module, the mask prompt generator, and the SAM 2 model. Given an input remote sensing image \mathcal{I} and its associated textual description $\mathcal{E} = \{e_l\}_{l=1}^L$, where L represents the number of words, the union encoder processes both modalities to extract a multimodal [CLS] token, visual patch embeddings, and textual embeddings. The SAM 2 image encoder, which incorporates the bidirectional hierarchical fusion module, further refines the extracted image features by leveraging textual information. Next, the mask prompt generator utilizes the visual patch embeddings and the multimodal [CLS] token to produce a pseudo-mask estimate for the target object. This prior mask, along with the multimodal [CLS] token, acts as a guiding signal for SAM 2. Ultimately, the SAM 2 decoder synthesizes the extracted image features and generated prompts to produce high-precision segmentation masks, while the text-guided boundary loss constrains the accuracy of object contours.

3.2. Feature Extraction

For the RRSIS task, aligning the visual and linguistic modalities is vital. We adopt the union BEiT-3 [29] encoder to simultaneously process the visual and textual features, in line with the approaches in [37, 42]. Each input frame $I_u \in \mathbb{R}^{H_u \times W_u \times 3}$ is divided into non-overlapping patches $P_v \in \mathbb{R}^{N_p \times (p^2 \times 3)}$, which are then projected into a D -dimensional space, yielding $P_v \in \mathbb{R}^{N_p \times D}$. Here, $N_p = \frac{H_u \times W_u}{p^2}$, and D represents the embedding dimension. A visual class token $V_{cls} \in \mathbb{R}^{1 \times D}$ is prepended, along with learnable positional embeddings $V_{pos} \in \mathbb{R}^{(N_p+1) \times D}$, to form the final visual representation $V_0 \in \mathbb{R}^{(N_p+1) \times D}$. Concurrently, the textual input of length L is tokenized using XLMRobertaTokenizer [4], yielding the tokenized sequence T_{seq} . A class token $T_{cls} \in \mathbb{R}^{1 \times D}$ and end-of-sequence marker $T_{eos} \in \mathbb{R}^{1 \times D}$ are appended, followed by positional embeddings $T_{pos} \in \mathbb{R}^{N_t \times D}$, where $N_t = L + 2$. The final union multimodal representation U_0 is obtained by concatenating the visual and text embeddings, i.e., $U_0 = \text{concat}(V_0, T_0)$. The above procedure is formally represented as:

$$\begin{aligned} V_0 &= [V_{cls}, P_v] + V_{pos}, \\ T_0 &= [T_{cls}, T_{seq}, T_{eos}] + T_{pos}, \\ U_0 &= [V_0; T_0] \in \mathbb{R}^{(N_p+N_t+1) \times D}. \end{aligned} \quad (1)$$

After multimodal fusion through multiple attention blocks, the joint visual-text embedding is passed into modality-specific FFNs for both vision and text processing. Ultimately, we obtain the union visual-text embeddings $U \in \mathbb{R}^{(N_p+N_t+1) \times D}$, which are then decomposed into a multimodal [CLS] token $V_{cls} \in \mathbb{R}^{1 \times D}$, visual patch embeddings $V \in \mathbb{R}^{N_p \times D}$, and text embeddings $T \in \mathbb{R}^{N_t \times D}$.

Subsequently, the SAM 2 image encoder, in conjunction

with the proposed bidirectional hierarchical fusion module, encodes the input image $I_s \in \mathbb{R}^{H_s \times W_s \times 3}$. It extracts a set of hierarchical multi-scale features for mask production, while the final-layer image feature $F_n \in \mathbb{R}^{\frac{H_s}{16} \times \frac{W_s}{16} \times C}$ serves as the input for the subsequent decoding process. Here, C , H_s and W_s represent the channel number, height, and width of the SAM 2 image encoder, respectively.

3.3. Bidirectional Hierarchical Fusion Module

Although SAM 2 demonstrates powerful segmentation capabilities for natural images, it struggles to achieve accurate segmentation for remote sensing images with more complex scenes. Inspired by MSA [31], a straightforward approach is to incorporate linear layers into the SAM 2 image encoder to enhance its adaptability to remote sensing images. However, for the RRSIS task, integrating textual information during SAM 2’s image encoding process could make the model more sensitive to referred objects. To address this, we designed a bidirectional hierarchical fusion module and embedded it into SAM 2 image encoder, enabling the visual feature of SAM 2 to better adapt to remote sensing scenes and the referring text, thereby achieving more precise segmentation.

As illustrated in Fig. 3, our bidirectional hierarchical fusion module begins with the preprocessed SAM 2 image feature F_i of the current layer being projected to a lower dimensionality through a linear layer and an activation function. Simultaneously, the text feature T_i of the current layer is also projected to match the dimensionality of the image feature using a linear layer. Subsequently, the image and text features are utilized as query embeddings and key-value pairs, respectively, and undergo cross-attention interaction to capture modality-specific dependencies. The resulting features are then integrated with the pre-interaction representations through element-wise addition. Following this, linear layers are used to restore the dimensionality of both the image and text features. The above process can be expressed by the following equation:

$$\begin{aligned} F'_i &= \sigma(\text{Linear}(F_i)), T'_i = \text{Linear}(T_i), \\ F''_i &= \text{MHCA}(F'_i, T'_i) + F'_i, \\ T''_i &= \text{MHCA}(T'_i, F'_i) + T'_i, \end{aligned} \quad (2)$$

where σ denotes the activation function GeLU and MHCA represents the multi-head cross-attention layer.

To preserve textual integrity during visual enhancement, the text feature is weighted and summed with its pre-interaction representation. Meanwhile, after skip-connection, the visual feature is summed with the original image feature F_{in} of the current layer, then separately processed by the MLP branch and the linear branch, followed by weighted fusion. The entire process is depicted as follows:

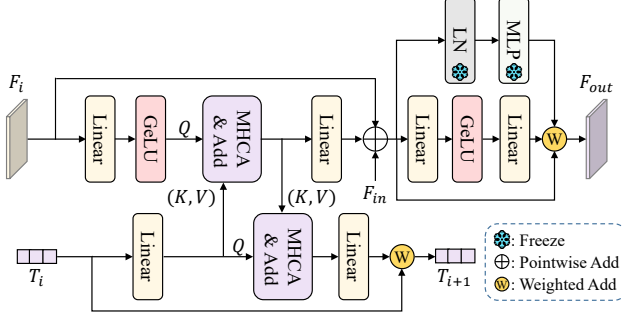


Figure 3. The structure of the bidirectional hierarchical fusion module.

$$\begin{aligned}
T_{i+1} &= (1 - \alpha_t)T_i + \alpha_t \text{Linear}(T_i''), \\
F_i''' &= F_{in} + \text{Linear}(F_i'') + F_i, \\
F_{out} &= F_i''' + \text{MLP}(\text{LN}(F_i''')) + \\
&\quad \alpha_i \text{Linear}(\sigma(\text{Linear}(F_i'''))),
\end{aligned} \tag{3}$$

here, α_t represents the text weighting coefficient, F_{out} denotes the image feature output to the next layer, and α_i represents the image weighting coefficient.

After feature encoding, the original text feature T encoded by the union encoder is used to further guide the visual feature F at the high-level. Specifically, the visual feature acts as query and interacts with the text feature as key-value pairs through multi-head cross-attention. The resulting feature is then element-wise multiplied with the visual feature before interaction. The process is as shown in the following equation:

$$F_{en} = \text{MHCA}(F, T) * F, \tag{4}$$

subsequently, the obtained text-guided hierarchical feature F_{en} is input into the SAM 2 decoder for accurate decoding.

3.4. Mask Prompt Generator

Although the SAM 2 image feature has been hierarchically guided by text features using the bidirectional hierarchical fusion module, further providing pixel-level semantic guidance could offer finer-grained textual information. Given the excellent semantic alignment between the visual embeddings V and the textual embeddings T in the joint encoding process, we propose combining the multimodal [CLS] token with visually aligned embeddings that are well-aligned with text. This combination generates a multimodal pseudo-mask prior, which provides pixel-level guidance for the SAM 2 decoding process.

As illustrated in Fig. 2, we first employ the multimodal [CLS] token V_{cls} as query and the visual embeddings V as key-value pairs for cross-attention computation. The interaction result is then element-wise multiplied with the

multimodal [CLS] token to further align the multimodal token with visual information. Subsequently, the visual embeddings are reshaped into feature maps with dimensions $\frac{H_u}{p} \times \frac{W_u}{p}$, and the multimodal token is passed through a linear layer and broadcasted to match the shape of the visual embeddings. After element-wise multiplication, the result is input into the mask generator, composed of MLP layers, to produce the pseudo-mask $M_p \in \mathbb{R}^{\frac{H_u}{p} \times \frac{W_u}{p}}$ that is well-aligned with multimodal information. The formal description of this process is provided as follows:

$$\begin{aligned}
V_{cls}' &= \text{MHCA}(V_{cls}, V), \\
V' &= R(V) * \text{Linear}(V_{cls}'), \\
M_p &= \text{MLP}(V'),
\end{aligned} \tag{5}$$

where MHCA represents the multi-head cross-attention layer, and $R(\cdot)$ denotes the reshape operation.

The pseudo-mask M_p is subsequently upsampled to dimensions H_s and W_s using linear interpolation, to match the feature size of the SAM 2 decoder. This upsampled pseudo-mask is subsequently fed as the dense prompt into the SAM 2 prompt encoder.

3.5. SAM 2 Prompt Encoder and Mask Decoder

The prompt encoder in RS2-SAM 2 accepts two types of inputs: the dense prompt M_p derived from the mask prompt generator and the sparse prompt V_{cls} produced by the union encoder. Following an approach similar to EVF-SAM [42], the [CLS] token V_{cls} is passed through a token MLP and then combined with sparse embeddings initialized to zero. To ensure compatibility, the pixel-level prompt M_p is adjusted to the spatial dimensions of SAM 2 features before being input as the dense spatial information into the mask decoder.

Within the SAM 2 mask decoder, both sparse object-level and dense pixel-level prompts are used. The sparse input is combined with object tokens to formulate queries for the decoder, while the dense pixel-level prompt, serving as the mask prior, is element-wise added to SAM 2 visual features to facilitate direct decoding from high-resolution feature representations.

3.6. Training Loss

RS2-SAM 2 utilizes a comprehensive loss function akin to that proposed in [19] to regulate the predicted mask, formulated as follows:

$$\mathcal{L} = \lambda_{ce} \mathcal{L}_{ce} + \lambda_{dice} \mathcal{L}_{dice} + \lambda_{tbl} \mathcal{L}_{tbl}, \tag{6}$$

where \mathcal{L}_{ce} corresponds to the cross-entropy loss, \mathcal{L}_{dice} denotes the DICE loss [22], and \mathcal{L}_{tbl} signifies the text-guided boundary loss, a loss function we designed that uses text-weighted constraints to predict mask boundaries.

Text-guided Boundary Loss. In the RRSIS task, unlike natural images, the target objects often exhibit low visual distinguishability from the background, making the boundaries of remote sensing targets less distinct. To address this, we introduce a text-guided boundary loss function L_{tbl} to constrain the predicted mask boundaries. Specifically, we first compute the difference between each pixel value and its neighboring pixel value in both horizontal and vertical directions to obtain the gradient, which serves as an indicator for boundary detection. Then, we abstract the text embeddings T into sentence embeddings T_s , reduce their dimensionality to a single scalar through a linear layer, and expand it to match the size of the mask as a text-guided weighting factor for the boundary gradient. Finally, we measure the boundary similarity between the predicted mask and the ground truth mask under the guidance of the text weights by MSE loss:

$$\begin{aligned} \nabla_{pre} &= Absd_h(M_{pre}) + Absd_v(M_{pre}) \\ \nabla_{gt} &= Absd_h(M_{gt}) + Absd_v(M_{gt}) \\ \mathcal{L}_{tbl} &= \frac{1}{N} \sum_{i=1}^N (\text{Linear}(T_s)(\nabla_{pre_i} - \nabla_{gt_i}))^2 \end{aligned} \quad (7)$$

where $Absd_h$ and $Absd_v$ represent the absolute differences between adjacent pixels in the horizontal and vertical directions, respectively, while ∇ denotes the gradient and N is the number of all pixels.

4. Experiments

4.1. Datasets and Metrics

Datasets. The experiments are performed on two key RRSIS datasets: RefSegRS [38] and RRSIS-D [19]. The RefSegRS dataset is the first remote sensing referring segmentation dataset, consisting of 2172 images for training, 413 images for validation, and 1817 images for testing. Each image in the dataset has a resolution of 512×512. RRSIS-D is a widely recognized and large-scale dataset in the field of RRSIS, containing 12181 samples in the training set, 1740 samples in the validation set and 3481 samples in the test set. The resolution of each image is 800×800.

Evaluation Metrics. In accordance with the evaluation protocol established in [19], we assess our model using several metrics, including precision at various IoU thresholds (Pr@0.5 to Pr@0.9), mean Intersection-over-Union (mIoU), and overall Intersection-over-Union (oIoU). These metrics are computed on the validation and test sets of both RefSegRS and RRSIS-D datasets.

4.2. Implementation Details

Model Settings. We initialize the key modules of SAM 2 and the union encoder using pre-trained weights from SAM

2-Hiera-Large [24] and BEiT-3-Large [29]. For feature extraction, each image is resized to 1024×1024 and 224×224, which are then fed into the SAM 2 image encoder with an output dimension of $C = 256$ and the union encoder with an output dimension of $D = 1024$. Unlike SAM 2’s full capabilities, we do not employ its memory mechanism, focusing exclusively on image processing. In the bidirectional hierarchical fusion module, we set the text weight coefficient α_t to 0.2 and the image weight coefficient α_i to 0.5.

Training Details. Experiments are conducted on 8 NVIDIA GeForce RTX 4090 GPUs. The experiment adopts a setup similar to [14], with training conducted for 60 epochs on the RefSegRS [38] dataset and 40 epochs on the RRSIS-D [19] dataset. We use the AdamW optimizer [21] with a unified batch size of 1. The learning rates for models on RefSegRS and RRSIS-D dataset are set to 5e-5 and 1e-5, respectively. To facilitate the adaptation of our designed modules to remote sensing data, the learning rates for bidirectional hierarchical fusion module and mask prompt generator are assigned as 1e-4 on RefSegRS dataset and 5e-5 on RRSIS-D dataset. All learning rates are reduced to 0.1 times their original values during the last 10 epochs. The weighting coefficients for various loss functions are defined as follows: $\lambda_{dice} = 0.1$, $\lambda_{ce} = 1$, and $\lambda_{tbl} = 0.2$.

4.3. Comparison with State-of-the-Art Methods

RefSegRS dataset. We conduct a comprehensive comparison between our method, RS2-SAM 2, and several state-of-the-art approaches on the RefSegRS [38] dataset. The results of the comparison are reported in Tab. 1. It can be observed that our RS2-SAM 2 achieves 88.03% oIoU and 85.21% mIoU on the validation set, surpassing the previous best method, RMSIN, by 5.62% in oIoU and 11.37% in mIoU. On the test set, it reaches 80.87% oIoU and 73.90% mIoU, outperforming FIANet [14] by 2.55% and 5.23%, respectively. Moreover, the Pr metric exhibits significant improvements across all thresholds, particularly at Pr@0.7, Pr@0.8, and Pr@0.9, demonstrating the model’s strong multimodal segmentation capabilities.

RRSIS-D dataset. We also conduct comparative experiments between our RS2-SAM 2 and existing methods such as LGCE [38], LAVT [35], EVF-SAM [42] and RMSIN [19], etc., on the RRSIS-D [19] dataset, with results documented in Tab. 2. On this dataset, our method achieves the best performance, surpassing the current state-of-the-art method RMSIN on the validation set by 4.59% in Pr@0.5, 5.86% in Pr@0.6, 6.44% in Pr@0.7, 5.28% in Pr@0.8, 5.97% in Pr@0.9, 1.89% in oIoU, and 3.71% in mIoU. It also significantly outperformed existing methods on the test set, demonstrating its strong capability in remote sensing object segmentation.

Fig. 4 illustrates the visual comparison between our model and RMSIN [19] on the RRSIS-D dataset. The re-

Table 1. Comparison with state-of-the-art methods on the RefSegRS dataset. The top-performing results are presented in bold, while the second-best results are underlined. Our model achieves the best performance across all metrics.

| Method | Reference | Pr@0.5 | | Pr@0.6 | | Pr@0.7 | | Pr@0.8 | | Pr@0.9 | | oIoU | | mIoU | |
|--------------|-----------|--------------|--------------|--------------|--------------|--------------|--------------|--------------|--------------|--------------|--------------|--------------|--------------|--------------|--------------|
| | | Val | Test | Val | Test | Val | Test | Val | Test | Val | Test | Val | Test | Val | Test |
| BRINet [6] | CVPR'20 | 36.86 | 20.72 | 35.53 | 14.26 | 19.93 | 9.87 | 10.66 | 2.98 | 2.84 | 1.14 | 61.59 | 58.22 | 38.73 | 31.51 |
| LSCM [8] | ECCV'20 | 56.82 | 31.54 | 41.24 | 20.41 | 21.85 | 9.51 | 12.11 | 5.29 | 2.51 | 0.84 | 62.82 | 61.27 | 40.59 | 35.54 |
| CMPC [7] | CVPR'20 | 46.09 | 32.36 | 26.45 | 14.14 | 12.76 | 6.55 | 7.42 | 1.76 | 1.39 | 0.22 | 63.55 | 55.39 | 42.08 | 40.63 |
| CMSA [36] | CVPR'19 | 39.24 | 28.07 | 38.44 | 20.25 | 20.39 | 12.71 | 11.79 | 5.61 | 1.52 | 0.83 | 65.84 | 64.53 | 43.62 | 41.47 |
| RRN [15] | CVPR'18 | 55.43 | 30.26 | 42.98 | 23.01 | 23.11 | 14.87 | 13.72 | 7.17 | 2.64 | 0.98 | 69.24 | 65.06 | 50.81 | 41.88 |
| EVF-SAM [42] | Arxiv'24 | 57.77 | 35.17 | 37.59 | 22.34 | 16.24 | 9.36 | 4.87 | 2.86 | 1.86 | 0.39 | 59.61 | 55.51 | 46.98 | 36.64 |
| CMPC+ [18] | TPAMI'21 | 56.84 | 49.19 | 37.59 | 28.31 | 20.42 | 15.31 | 10.67 | 8.12 | 2.78 | 2.55 | 70.62 | 66.53 | 47.13 | 43.65 |
| CARIS [20] | ACM MM'23 | 68.45 | 45.40 | 47.10 | 27.19 | 25.52 | 15.08 | 14.62 | 8.87 | 3.71 | 1.98 | 75.79 | 69.74 | 54.30 | 42.66 |
| CRIS [30] | CVPR'22 | 53.13 | 35.77 | 36.19 | 24.11 | 24.36 | 14.36 | 11.83 | 6.38 | 2.55 | 1.21 | 72.14 | 65.87 | 53.74 | 43.26 |
| LAVT [35] | CVPR'22 | 80.97 | 51.84 | 58.70 | 30.27 | 31.09 | 17.34 | 15.55 | 9.52 | 4.64 | 2.09 | 78.50 | 71.86 | 61.53 | 47.40 |
| RIS-DMMI [5] | CVPR'23 | 86.17 | 63.89 | 74.71 | 44.30 | 38.05 | 19.81 | 18.10 | 6.49 | 3.25 | 1.00 | 74.02 | 68.58 | 65.72 | 52.15 |
| LGCE [38] | TGRS'24 | 90.72 | 73.75 | 86.31 | 61.14 | 71.93 | 39.46 | <u>32.95</u> | 16.02 | <u>10.21</u> | 5.45 | 83.56 | 76.81 | 72.51 | 59.96 |
| RMSIN [19] | CVPR'24 | <u>93.97</u> | 79.20 | <u>89.33</u> | 65.99 | <u>74.25</u> | 42.98 | 29.70 | 16.51 | 7.89 | 3.25 | 82.41 | 75.72 | <u>73.84</u> | 62.58 |
| FIANet [14] | TGRS'24 | - | <u>84.09</u> | - | <u>77.05</u> | - | 61.86 | - | 33.41 | - | 7.10 | - | <u>78.32</u> | - | 68.67 |
| RS2-SAM 2 | - | 95.36 | 84.31 | 94.90 | 79.42 | 92.58 | 70.89 | 83.76 | 55.70 | 36.66 | 21.19 | 88.03 | 80.87 | 85.21 | 73.90 |

Table 2. Comparison with state-of-the-art methods on the RRSIS-D dataset. The top-performing results are presented in bold, while the second-best results are underlined. Our model achieves the best performance across all metrics.

| Method | Reference | Pr@0.5 | | Pr@0.6 | | Pr@0.7 | | Pr@0.8 | | Pr@0.9 | | oIoU | | mIoU | |
|--------------|-----------|--------------|--------------|--------------|--------------|--------------|--------------|--------------|--------------|--------------|--------------|--------------|--------------|--------------|--------------|
| | | Val | Test | Val | Test | Val | Test | Val | Test | Val | Test | Val | Test | Val | Test |
| RRN [15] | CVPR'18 | 51.09 | 51.07 | 42.47 | 42.11 | 33.04 | 32.77 | 20.80 | 21.57 | 6.14 | 6.37 | 66.53 | 66.43 | 46.06 | 45.64 |
| CMSA [36] | CVPR'19 | 55.68 | 55.32 | 48.04 | 46.45 | 38.27 | 37.43 | 26.55 | 25.39 | 9.02 | 8.15 | 69.68 | 69.39 | 48.85 | 48.54 |
| LSCM [8] | ECCV'20 | 57.12 | 56.02 | 48.04 | 46.25 | 37.87 | 37.70 | 26.37 | 25.28 | 7.93 | 8.27 | 69.28 | 69.05 | 50.36 | 49.92 |
| CMPC [7] | CVPR'20 | 57.93 | 55.83 | 48.85 | 47.40 | 38.50 | 36.94 | 25.28 | 25.45 | 9.31 | 9.19 | 70.15 | 69.22 | 50.41 | 49.24 |
| BRINet [6] | CVPR'20 | 58.79 | 56.90 | 49.54 | 48.77 | 39.65 | 39.12 | 28.21 | 27.03 | 9.19 | 8.73 | 70.73 | 69.88 | 51.14 | 49.65 |
| CMPC+ [18] | TPAMI'21 | 59.19 | 57.65 | 49.36 | 47.51 | 38.67 | 36.97 | 25.91 | 24.33 | 8.16 | 7.78 | 70.14 | 68.64 | 51.41 | 50.24 |
| LGCE [38] | TGRS'24 | 68.10 | 67.65 | 60.52 | 61.53 | 52.24 | 51.45 | 42.24 | 39.62 | 23.85 | 23.33 | 76.68 | 76.34 | 60.16 | 59.37 |
| RIS-DMMI [5] | CVPR'23 | 70.40 | 68.74 | 63.05 | 60.96 | 54.14 | 50.33 | 41.95 | 38.38 | 23.85 | 21.63 | 77.01 | 76.20 | 60.72 | 60.12 |
| LAVT [35] | CVPR'22 | 69.54 | 69.52 | 63.51 | 63.63 | 53.16 | 53.29 | 43.97 | 41.60 | 24.25 | 24.94 | 77.59 | 77.19 | 61.46 | 61.04 |
| EVF-SAM [42] | Arxiv'24 | 73.51 | 72.16 | 67.87 | 66.50 | <u>58.33</u> | <u>56.59</u> | <u>46.15</u> | <u>43.92</u> | <u>25.92</u> | <u>25.48</u> | 76.32 | 76.77 | 64.03 | 62.75 |
| FIANet [14] | TGRS'24 | - | 74.46 | - | 66.96 | - | 56.31 | - | 42.83 | - | 24.13 | - | 76.91 | - | 64.01 |
| RMSIN [19] | CVPR'24 | 74.66 | 74.26 | 68.22 | 67.25 | 57.41 | 55.93 | 45.29 | 42.55 | 24.43 | 24.53 | <u>78.27</u> | <u>77.79</u> | 65.10 | 64.20 |
| RS2-SAM 2 | - | 79.25 | 77.56 | 74.08 | 72.34 | 63.85 | 61.76 | 50.57 | 47.92 | 30.40 | 29.73 | 80.16 | 78.99 | 68.81 | 66.72 |

sults clearly indicate that RS2-SAM 2 consistently outperforms RMSIN, particularly in terms of accurate target localization, reliable mask prediction, and boundary precision.

4.4. Model Analysis

In this section, we perform extensive ablation studies to analyze the impact of the essential components in our RS2-SAM 2 framework, as well as the effects of different model configurations. The experiments are conducted on the test dataset of RefSegRS [38].

Components Analysis. To investigate the impact of key components in our model, we first construct a baseline model consisting solely of SAM 2 and the union encoder. As shown in Tab. 3, when the text-guided boundary loss (\mathcal{L}_{tbl}) is incorporated during training, the model achieves 38.63% mIoU and 57.36% oIoU, surpassing the baseline by 1.99% and 1.85%, respectively. Subsequently, on top of the

Table 3. Ablation study of different components of RS2-SAM 2 on RefSegRS test set.

| Method | \mathcal{L}_{tbl} | MMP | DHF | Pr@0.5 | Pr@0.7 | Pr@0.9 | mIoU | oIoU |
|-----------|---------------------|-----|-----|--------------|--------------|--------------|--------------|--------------|
| Baseline | | | | 35.17 | 9.36 | 0.39 | 36.64 | 55.51 |
| RS2-SAM 2 | ✓ | | | 39.79 | 12.49 | 0.39 | 38.63 | 57.36 |
| RS2-SAM 2 | ✓ | ✓ | | 71.00 | 43.42 | 3.96 | 60.20 | 70.89 |
| RS2-SAM 2 | ✓ | | ✓ | 81.89 | 61.86 | 7.10 | 68.71 | 78.36 |
| RS2-SAM 2 | ✓ | ✓ | ✓ | 84.31 | 70.89 | 21.19 | 73.90 | 80.87 |

model with \mathcal{L}_{tbl} , we add the mask prompt generator (MPG), which results in the RS2-SAM 2 achieving 60.20% mIoU and 70.89% oIoU, an improvement of 21.57% and 13.53% over the previous model. When the bidirectional hierarchical fusion module (BHF) is added to the baseline model

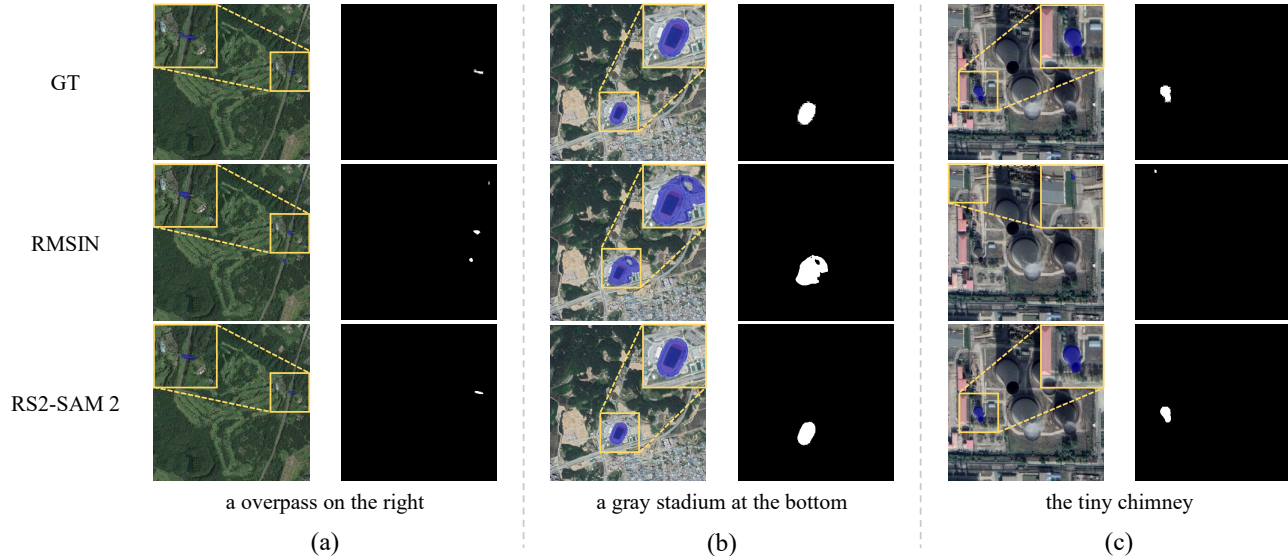


Figure 4. Visualization result on RRSIS-D. Compared to RMSIN [19], RS2-SAM 2 demonstrates superior capability in handling local details and boundary regions.

Table 4. Model analysis of different settings in RS2-SAM 2.

| Method | Settings | Pr@0.5 | Pr@0.7 | Pr@0.9 | mIoU | oIoU |
|---------------------------------|----------|--------------|--------------|--------------|--------------|--------------|
| Interaction Form of MPG | | | | | | |
| RS2-SAM 2 | w/o MHCA | 83.71 | 67.64 | 16.79 | 71.59 | 79.89 |
| RS2-SAM 2 | w MHCA | 84.31 | 70.89 | 21.19 | 73.90 | 80.87 |
| Structure of BHFMM layer | | | | | | |
| RS2-SAM 2 | Linear | 81.01 | 61.42 | 6.77 | 68.19 | 77.39 |
| RS2-SAM 2 | Uni | 81.23 | 63.84 | 14.14 | 70.10 | 78.93 |
| RS2-SAM 2 | Bi | 84.31 | 70.89 | 21.19 | 73.90 | 80.87 |
| Components of BHFMM | | | | | | |
| RS2-SAM 2 | w/o BC | 79.97 | 58.17 | 11.61 | 67.61 | 77.54 |
| RS2-SAM 2 | w/o BL | 72.21 | 43.48 | 4.79 | 61.08 | 72.33 |
| RS2-SAM 2 | w BC&BL | 84.31 | 70.89 | 21.19 | 73.90 | 80.87 |

with \mathcal{L}_{tbl} , the model shows a further increase of 30.08% in mIoU and 21.00% in oIoU, further validating the superiority of this module. Finally, when all components are integrated, our RS2-SAM 2 achieves the best performance, with a mIoU of 73.90% and an oIoU of 80.87%.

Mask Prompt Generator. In this section, we explore different interaction forms within the mask prompt generator (MPG), with results presented in Tab. 4. When the multi-head cross-attention (MHCA) between the multimodal token V_{cls} and visual embeddings V is omitted, the performance of RS2-SAM 2 drops by 2.31% in mIoU and 0.98% in oIoU. These findings underscore the importance of further strengthening the semantic connections between the multimodal token and visual embeddings during the multimodal mask prompt generation process.

Bidirectional Hierarchical Fusion Module. The impact of different settings of the bidirectional hierarchical fusion module (BHFMM) is also noteworthy. First, we examine how the structure of the BHFMM layer during feature encoding affects the model’s performance. One simple approach is to use a linear layer structure similar to the adapter, without interacting with text feature, referred to as “Linear”. Another approach is to enhance visual feature using only text feature, without back-propagating visual information, referred to as “Uni”. The third approach is bidirectional enhancement of both text and visual features, referred to as “Bi”. The experimental results in Tab. 4 show that the layer-by-layer bidirectional enhancement of text and visual features is more beneficial for imparting linguistic information to the visual feature. This enables refined linguistic enhancement of the visual feature from low-level to high-level, leading to more accurate segmentation of remote sensing objects.

Additionally, we investigate the impact of BHFMM components on segmentation performance by setting up experiments where the BHFMM cross-attention (BC) after encoding and the BHFMM layer (BL) without the encoder are removed. The results in Tab. 4 indicate that both interactions during and after encoding are essential. The hierarchical interaction combining both can help the model understand text features from a global to a local perspective, enhancing its pixel-level understanding of text.

5. Conclusion

In this paper, we present RS2-SAM 2, an advanced end-to-end framework designed to enhance SAM 2 for RRSIS.

Our approach leverages a union encoder to jointly encode visual and textual features, producing semantically aligned visual-text embeddings and multimodal class tokens. To effectively integrate spatial and textual information, we introduce a bidirectional hierarchical fusion module, which incorporates textual semantics and spatial context both during and after encoding, enabling a hierarchical refinement from global to local levels. Additionally, a mask prompt generator generates multimodal mask as dense prompt, improving the segmentation of visually indistinct objects by providing stronger pixel-level guidance. To further enhance boundary precision, we propose a text-guided boundary loss, which refines segmentation results by computing text-weighted boundary gradient differences. Extensive experiments on multiple RRSIS benchmarks demonstrate the superiority of RS2-SAM 2 over state-of-the-art methods, validating the effectiveness of our proposed modules.

References

- [1] Tianrun Chen, Ankang Lu, Lanyun Zhu, Chaotao Ding, Chunan Yu, Deyi Ji, Zejian Li, Lingyun Sun, Papa Mao, and Ying Zang. Sam2-adapter: Evaluating & adapting segment anything 2 in downstream tasks: Camouflage, shadow, medical image segmentation, and more. *arXiv preprint arXiv:2408.04579*, 2024. 2
- [2] Yangming Cheng, Liulei Li, Yuanyou Xu, Xiaodi Li, Zongxin Yang, Wenguan Wang, and Yi Yang. Segment and track anything. *arXiv preprint arXiv:2305.06558*, 2023. 3
- [3] Zhiheng Cheng, Qingyue Wei, Hongru Zhu, Yan Wang, Liangqiong Qu, Wei Shao, and Yuyin Zhou. Unleashing the potential of sam for medical adaptation via hierarchical decoding. In *Proceedings of the IEEE/CVF Conference on Computer Vision and Pattern Recognition*, pages 3511–3522, 2024. 3
- [4] A Conneau. Unsupervised cross-lingual representation learning at scale. *arXiv preprint arXiv:1911.02116*, 2019. 4
- [5] Yutao Hu, Qixiong Wang, Wenqi Shao, Enze Xie, Zhenguo Li, Jungong Han, and Ping Luo. Beyond one-to-one: Rethinking the referring image segmentation. In *Proceedings of the IEEE/CVF International Conference on Computer Vision*, pages 4067–4077, 2023. 7
- [6] Zhiwei Hu, Guang Feng, Jiayu Sun, Lihe Zhang, and Huchuan Lu. Bi-directional relationship inferring network for referring image segmentation. In *Proceedings of the IEEE/CVF conference on computer vision and pattern recognition*, pages 4424–4433, 2020. 7
- [7] Shaofei Huang, Tianrui Hui, Si Liu, Guanbin Li, Yunchao Wei, Jizhong Han, Luoqi Liu, and Bo Li. Referring image segmentation via cross-modal progressive comprehension. In *Proceedings of the IEEE/CVF conference on computer vision and pattern recognition*, pages 10488–10497, 2020. 7
- [8] Tianrui Hui, Si Liu, Shaofei Huang, Guanbin Li, Sansi Yu, Faxi Zhang, and Jizhong Han. Linguistic structure guided context modeling for referring image segmentation. In *Computer Vision—ECCV 2020: 16th European Conference, Glasgow, UK, August 23–28, 2020, Proceedings, Part X 16*, pages 59–75. Springer, 2020. 7
- [9] Lei Ke, Mingqiao Ye, Martin Danelljan, Yu-Wing Tai, Chi-Keung Tang, Fisher Yu, et al. Segment anything in high quality. *Advances in Neural Information Processing Systems*, 36, 2024. 1
- [10] Alexander Kirillov, Eric Mintun, Nikhila Ravi, Hanzi Mao, Chloe Rolland, Laura Gustafson, Tete Xiao, Spencer Whitehead, Alexander C Berg, Wan-Yen Lo, et al. Segment anything. In *Proceedings of the IEEE/CVF International Conference on Computer Vision*, pages 4015–4026, 2023. 1, 3
- [11] Xin Lai, Zhuotao Tian, Yukang Chen, Yanwei Li, Yuhui Yuan, Shu Liu, and Jiaya Jia. Lisa: Reasoning segmentation via large language model. In *Proceedings of the IEEE/CVF Conference on Computer Vision and Pattern Recognition*, pages 9579–9589, 2024. 3
- [12] Meng Lan, Jing Zhang, Lefei Zhang, and Dacheng Tao. Learning to learn better for video object segmentation. In *Proceedings of the AAAI Conference on Artificial Intelligence*, pages 1205–1212, 2023. 3
- [13] Meng Lan, Fu Rong, Hongzan Jiao, Zhi Gao, and Lefei Zhang. Language query based transformer with multi-scale cross-modal alignment for visual grounding on remote sensing images. *IEEE Transactions on Geoscience and Remote Sensing*, 2024. 2
- [14] Sen Lei, Xinyu Xiao, Tianlin Zhang, Heng-Chao Li, Zhenwei Shi, and Qing Zhu. Exploring fine-grained image-text alignment for referring remote sensing image segmentation. *IEEE Transactions on Geoscience and Remote Sensing*, 2024. 3, 6, 7
- [15] Ruiyu Li, Kaican Li, Yi-Chun Kuo, Michelle Shu, Xiaojuan Qi, Xiaoyong Shen, and Jiaya Jia. Referring image segmentation via recurrent refinement networks. In *Proceedings of the IEEE Conference on Computer Vision and Pattern Recognition*, pages 5745–5753, 2018. 7
- [16] Haotian Liu, Chunyuan Li, Qingyang Wu, and Yong Jae Lee. Visual instruction tuning. *Advances in neural information processing systems*, 36, 2024. 3
- [17] Jiang Liu, Hui Ding, Zhaowei Cai, Yuting Zhang, Ravi Kumar Satzoda, Vijay Mahadevan, and R Manmatha. Polyformer: Referring image segmentation as sequential polygon generation. In *Proceedings of the IEEE/CVF conference on computer vision and pattern recognition*, pages 18653–18663, 2023. 1
- [18] Si Liu, Tianrui Hui, Shaofei Huang, Yunchao Wei, Bo Li, and Guanbin Li. Cross-modal progressive comprehension for referring segmentation. *IEEE Transactions on Pattern Analysis and Machine Intelligence*, 44(9):4761–4775, 2021. 7
- [19] Sihan Liu, Yiwei Ma, Xiaoqing Zhang, Haowei Wang, Jiayi Ji, Xiaoshuai Sun, and Rongrong Ji. Rotated multi-scale interaction network for referring remote sensing image segmentation. In *Proceedings of the IEEE/CVF Conference on Computer Vision and Pattern Recognition*, pages 26658–26668, 2024. 1, 2, 3, 5, 6, 7, 8

- [20] Sun-Ao Liu, Yiheng Zhang, Zhaofan Qiu, Hongtao Xie, Yongdong Zhang, and Ting Yao. Caris: Context-aware referring image segmentation. In *Proceedings of the 31st ACM International Conference on Multimedia*, pages 779–788, 2023. 7
- [21] Ilya Loshchilov and Frank Hutter. Decoupled weight decay regularization. In *ICLR*, 2018. 6
- [22] Fausto Milletari, Nassir Navab, and Seyed-Ahmad Ahmadi. V-net: Fully convolutional neural networks for volumetric medical image segmentation. In *Proceedings of the International Conference on 3D Vision (3DV)*, pages 565–571, 2016. 5
- [23] Hanoona Rasheed, Muhammad Maaz, Sahal Shaji, Abdelrahman Shaker, Salman Khan, Hisham Cholakkal, Rao M Anwer, Eric Xing, Ming-Hsuan Yang, and Fahad S Khan. Glamm: Pixel grounding large multimodal model. In *Proceedings of the IEEE/CVF Conference on Computer Vision and Pattern Recognition*, pages 13009–13018, 2024. 3
- [24] Nikhila Ravi, Valentin Gabeur, Yuan-Ting Hu, Ronghang Hu, Chaitanya Ryali, Tengyu Ma, Haitham Khedr, Roman Rädle, Chloe Rolland, Laura Gustafson, et al. Sam 2: Segment anything in images and videos. *arXiv preprint arXiv:2408.00714*, 2024. 1, 3, 6
- [25] Fu Rong, Meng Lan, Qian Zhang, and Lefei Zhang. Mpgsam 2: Adapting sam 2 with mask priors and global context for referring video object segmentation. *arXiv preprint arXiv:2501.13667*, 2025. 3
- [26] Chaitanya Ryali, Yuan-Ting Hu, Daniel Bolya, Chen Wei, Haoqi Fan, Po-Yao Huang, Vaibhav Aggarwal, Arkabandhu Chowdhury, Omid Poursaeed, Judy Hoffman, et al. Hiera: A hierarchical vision transformer without the bells-and-whistles. In *International conference on machine learning*, pages 29441–29454. PMLR, 2023. 2
- [27] Yuxi Sun, Shanshan Feng, Xutao Li, Yunming Ye, Jian Kang, and Xu Huang. Visual grounding in remote sensing images. In *Proceedings of the 30th ACM International Conference on Multimedia*, pages 404–412, 2022. 2
- [28] Di Wang, Jing Zhang, Bo Du, Minqiang Xu, Lin Liu, Dacheng Tao, and Liangpei Zhang. Samrs: Scaling-up remote sensing segmentation dataset with segment anything model. *Advances in Neural Information Processing Systems*, 36, 2024. 3
- [29] Wenhui Wang, Hangbo Bao, Li Dong, Johan Bjorck, Zhiliang Peng, Qiang Liu, Kriti Aggarwal, Owais Khan Mohammed, Saksham Singhal, Subhojit Som, et al. Image as a foreign language: Beit pretraining for vision and vision-language tasks. In *Proceedings of the IEEE/CVF Conference on Computer Vision and Pattern Recognition*, pages 19175–19186, 2023. 4, 6
- [30] Zhaoqing Wang, Yu Lu, Qiang Li, Xunqiang Tao, Yandong Guo, Mingming Gong, and Tongliang Liu. Cris: Clip-driven referring image segmentation. In *Proceedings of the IEEE/CVF conference on computer vision and pattern recognition*, pages 11686–11695, 2022. 1, 7
- [31] Junde Wu, Wei Ji, Yuanpei Liu, Huazhu Fu, Min Xu, Yanwu Xu, and Yueming Jin. Medical sam adapter: Adapting segment anything model for medical image segmentation. *arXiv preprint arXiv:2304.12620*, 2023. 4
- [32] Yunyang Xiong, Bala Varadarajan, Lemeng Wu, Xiaoyu Xiang, Fanyi Xiao, Chenchen Zhu, Xiaoliang Dai, Dilin Wang, Fei Sun, Forrest Iandola, et al. Efficientsam: Leveraged masked image pretraining for efficient segment anything. In *Proceedings of the IEEE/CVF Conference on Computer Vision and Pattern Recognition*, pages 16111–16121, 2024. 1, 3
- [33] Jinjin Xu, Liwu Xu, Yuzhe Yang, Xiang Li, Fanyi Wang, Yanchun Xie, Yi-Jie Huang, and Yaqian Li. u-llava: Unifying multi-modal tasks via large language model. *arXiv preprint arXiv:2311.05348*, 2023. 3
- [34] Cilin Yan, Haochen Wang, Shilin Yan, Xiaolong Jiang, Yao Hu, Guoliang Kang, Weidi Xie, and Efstratios Gavves. Visa: Reasoning video object segmentation via large language models. In *European Conference on Computer Vision*, pages 98–115. Springer, 2024. 3
- [35] Zhao Yang, Jiaqi Wang, Yansong Tang, Kai Chen, Hengshuang Zhao, and Philip HS Torr. Lavt: Language-aware vision transformer for referring image segmentation. In *Proceedings of the IEEE/CVF Conference on Computer Vision and Pattern Recognition*, pages 18155–18165, 2022. 1, 2, 6, 7
- [36] Linwei Ye, Mrigank Rochan, Zhi Liu, and Yang Wang. Cross-modal self-attention network for referring image segmentation. In *Proceedings of the IEEE/CVF conference on computer vision and pattern recognition*, pages 10502–10511, 2019. 7
- [37] Seonghoon Yu, Ilchae Jung, Byeongju Han, Taehoh Kim, Yunho Kim, Dongyoon Wee, and Jeany Son. A simple baseline with single-encoder for referring image segmentation. *arXiv preprint arXiv:2408.15521*, 2024. 4
- [38] Zhenghang Yuan, Lichao Mou, Yuansheng Hua, and Xiao Xiang Zhu. Rrsis: Referring remote sensing image segmentation. *IEEE Transactions on Geoscience and Remote Sensing*, 2024. 1, 2, 6, 7
- [39] Wenxi Yue, Jing Zhang, Kun Hu, Yong Xia, Jiebo Luo, and Zhiyong Wang. Surgicalsam: Efficient class promptable surgical instrument segmentation. In *Proceedings of the AAAI Conference on Artificial Intelligence*, pages 6890–6898, 2024. 3
- [40] Yang Zhan, Zhitong Xiong, and Yuan Yuan. Rsvg: Exploring data and models for visual grounding on remote sensing data. *IEEE Transactions on Geoscience and Remote Sensing*, 61: 1–13, 2023. 2, 3
- [41] Chaoning Zhang, Dongshen Han, Yu Qiao, Jung Uk Kim, Sung-Ho Bae, Seungkyu Lee, and Choong Seon Hong. Faster segment anything: Towards lightweight sam for mobile applications. *arXiv preprint arXiv:2306.14289*, 2023. 1, 3
- [42] Yuxuan Zhang, Tianheng Cheng, Rui Hu, Lei Liu, Heng Liu, Longjin Ran, Xiaoxin Chen, Wenyu Liu, and Xinggang Wang. Evf-sam: Early vision-language fusion for text-prompted segment anything model. *arXiv preprint arXiv:2406.20076*, 2024. 2, 3, 4, 5, 6, 7
- [43] Zihan Zhong, Zhiqiang Tang, Tong He, Haoyang Fang, and Chun Yuan. Convolution meets lora: Parameter efficient finetuning for segment anything model. *arXiv preprint arXiv:2401.17868*, 2024. 3